First-principles calculation of the indentation strength of FeB_4

Bing Li,[1] Hong Sun,[1,*] and Changfeng Chen[2,†]

[1]*Department of Physics and Astronomy and Key Laboratory of Artificial Structures and Quantum Control (Ministry of Education), Shanghai Jiao Tong University, Shanghai 200240, China*

[2]*Department of Physics and High Pressure Science and Engineering Center, University of Nevada, Las Vegas, Nevada 89154, USA*

(Received 15 March 2014; revised manuscript received 29 May 2014; published 21 July 2014)

A recent experiment [H. Y. Gou *et al.*, Phys. Rev. Lett. **111**, 157002 (2013)] reported a measured Vickers hardness of over 60 GPa for FeB_4, placing it as a superhard material far above all other similar ultrahard transition-metal borides, such as ReB_2, WB_4, and especially CrB_4, which has the same crystalline structure as that of FeB_4 but a much lower measured Vickers hardness of around 23 GPa. This result, however, is contradicted by theoretical calculations that predict a smaller shear modulus for FeB_4 than that of CrB_4, indicating that FeB_4 is softer than CrB_4. Here we report first-principles calculations that aim to understand the stress response of FeB_4 under indentation loadings and examine whether there exists a strain-stiffening effect that might enhance the indentation strength. Our results show that there is no strain stiffening in FeB_4; instead, the normal pressure beneath the indenter drives a lateral structural expansion which further stretches and weakens the boron-boron and boron-iron bonds in addition to that caused by the shear deformation in Vickers indentation tests. This effect leads to a considerably reduced strength of FeB_4, producing an ideal (i.e., an upper bound) indentation strength of 17 GPa that is lower than that (27 GPa) predicted for CrB_4. The present results suggest that FeB_4 is unlikely to be superhard and further experimental investigation is needed to clarify this issue.

DOI: 10.1103/PhysRevB.90.014106 PACS number(s): 62.20.−x, 81.40.Jj, 61.50.Ah

I. INTRODUCTION

Searching for materials with exceptional physical properties is an important research topic in condensed matter physics and materials science. The recently synthesized iron-boride phase, FeB_4 [1], represents an exciting case study. This Fe-based superconductor with a phonon mediated superconducting mechanism [1,2] is also reported to be superhard with an exceptionally high Vickers hardness exceeding 60 GPa [1], which is well above those (20–30 GPa) of all known iron borides, which find wide applications as coating materials that enhance the strength and hardness of steel tools. They belong to a category of ultraincompressible and ultrahard materials consisting of small, light covalent elements (B, C, N, O) and large, electron-rich transition metals (Cr, Mn, Ru, W, Re, Os, Fe, ...). These materials provide a low-cost alternative to traditional superhard materials such as diamond and cubic boron nitride that require expensive high-temperature and high-pressure synthesis conditions. The covalent elements can form strong and directional covalent bonds with the transition metals, while the high density of valence electrons from the transition metals prevent the lattice structures from being squeezed together, both of which enhance the resistance of the transition-metal light-element compounds against large plastic (bulk and shear) deformation and lead to increased hardness. Various transition-metal light-element compounds have been successfully synthesized, among which transition-metal boron (TM-B) compounds, such as OsB_2 [3], ReB_2 [4–9], RuB_2 [7], WB_4 [7,10–12], and CrB_4 [13,14], attracted special attention for their high hardness due to the high content of boron. However, the measured (Vickers) hardnesses of all these TM-B compounds are less than 40 GPa. The reported anomalously high hardness of FeB_4 (>60 GPa) [1] represents a strong deviation from the mechanical properties established for the entire class of TM-B compounds. This result is particularly puzzling since the elastic shear modulus of FeB_4 is lower than that of the isostructural CrB_4 [15], which indicates that FeB_4 should be softer than CrB_4 that has a measured Vickers hardness of around 23 GPa [13,14]. Elastic coefficients, including bulk and shear modulus, measure the stress response of materials close to their equilibrium structures. A possible explanation for the unexpected high hardness of FeB_4 might be the strain-stiffening effect, namely, the enhancement of stiffness of materials under large structural deformations in indentation tests, which has been predicted for iron carbides, such as cementite Fe_3C [16]. It is thus essential to assess the stress response of FeB_4 under large shear deformation under Vickers indentation loading conditions, and the results would offer crucial insights into the atomistic mechanisms that determine the deformation and strength of FeB_4 and answer the question whether it really is an intrinsically superhard material. Our calculations show that FeB_4 follows the established trend for TM-B compounds without any strain induced stiffening, and it is not an intrinsic superhard material. At present, there is no other known mechanism capable of producing such dramatic hardness enhancement, and additional experimental studies of high-quality FeB_4 samples are needed to resolve this issue.

Recent advances in computational physics have made it possible to calculate the stress-strain relations of a crystal in various shear deformation directions under normal compressive pressure beneath an indenter. The lowest shear peak stress under an indenter, which is defined as the ideal indentation strength, gives the stress at which a perfect crystal becomes mechanically unstable under indentation [17–21]. Ideal indentation strength provides a more accurate description of material strength under indentation hardness tests than pure ideal shear strength that is calculated neglecting the normal

*Corresponding author: hsun@sjtu.edu.cn
†Corresponding author: chen@physics.unlv.edu

pressure beneath the indenter [22–33]. While material strength and hardness are controlled by many factors, such as defect nucleation and mobility, ideal shear (indentation) strength calculations can predict incipient plasticity in a crystal [34] and determine the lowest shear stress needed to destabilize a perfect crystal, thus setting an upper bound for material strength. The measured strength of high-quality samples can actually approach the calculated ideal strength [35,36]. This makes ideal shear (indentation) strength a benchmark quantity in assessing material strength and hardness; it is especially useful in a comparative study of different materials.

In this paper, we report on a systematic study of the ideal strength of FeB_4 under different loading conditions. We perform a comprehensive set of calculations to determine the ideal pure shear strength and ideal (Vickers) indentation strength of FeB_4. The obtained (Vickers) indentation strength value of FeB_4 is 16.6 GPa, which is significantly lower than the reported Vickers hardness (62 GPa) [1]. A detailed analysis of the bond breaking processes of a FeB_4 structure under indentation shear deformation shows that the uniaxial normal compressive pressure beneath the indenter causes a large lateral volume expansion that further stretches and weakens the boron-boron and iron-boron atomic bonds in addition to that caused by the shear deformation, leading to its reduced (Vickers) indentation strength. Our results on FeB_4 are similar to those observed in other TM-B compounds with different boron content and structure, such as ReB_2, WB_3, MoB_3, and CrB_4 [20,21,37]. The present work demonstrates that the deformation modes and stress response of FeB_4 are driven by the same atomistic mechanism and follow the same trend under large indentation shear strain as in other TM-B compounds, and our calculated indentation shear strength suggests that FeB_4 is unlikely to be superhard, as previously suggested [1].

II. COMPUTATIONAL METHOD

We performed calculations of ideal pure shear and indentation strength under a Vickers indenter using the VASP code [38] and adopting the projector augmented wave (PAW) potentials [39] with the generalized-gradient approximation (GGA) for the exchange-correlation energy with a plane-wave basis set. The GGA-PBE exchange-correlation functional proposed by Perdew, Burke, and Ernzerhof [40] was used. The total energy of the structure was minimized by relaxing the structural parameters using a conjugate gradient optimization method [41]. The total-energy and stress calculations used an orthorhombic unit cell with the space group *Pnnm* (No. 58) for FeB_4 determined previously [1,2]. A $9 \times 9 \times 11$ Monkhorst-Pack [42] k-point grid and a 600 eV energy cutoff were used in the calculations. The energy convergence of the calculation is on the order of 1 meV per atom, with the residual stresses and forces in the fully relaxed structures less than 0.1 GPa and 0.001 eV/Å. We performed spin-polarized calculations but found no magnetic moment for the equilibrium structure of FeB_4, consistent with the previous results [2]. All subsequent shear strength calculations were carried out using non-spin-polarized calculations. We also performed spin-polarized shear strength calculations for FeB_4 in selected (Vickers) indentation shear deformation directions. The results show that the magnetic moment of Fe atoms can appear and disappear during the deformation, but it does not have any appreciable impact on the shear strength of FeB_4. The quasistatic ideal indentation strength and relaxed loading path were determined using a method described previously [17–21]. In this method, the shape of the (deformed) unit cell, the positions of the atoms, and the relation between the shear stress σ_{zx} and shear strain ϵ_{zx} are determined completely at each step following a constrained atomic relaxation procedure, including the effect of the normal compressive pressure σ_{zz} by requiring that $\sigma_{zz} = \sigma_{zx} \tan\phi$ at each deformation step with ϕ the centerline-to-face angle of the Vickers indenter [see Fig. 3(h)]. The lowest peak stress in all the indentation shear directions determines the ideal indentation strength of the structure, at which the crystal structure starts to destabilize under the indenter. In a special case of setting $\sigma_{zz} = 0$, we recover the normal relaxation procedure used in previous calculations of pure ideal shear stresses [22–33] that neglect the effects of the normal compressive pressure beneath the indenter. As a test, we performed calculations for the equilibrium structures of FeB_4, and the obtained results of elastic constants, bulk and shear moduli, and Poisson's ratios (see Table I) are all in good agreement with the previously reported calculated results [15]. FeB_4 has a lower shear modulus and larger Poisson's ratio compared to CrB_4, which has the same structure as FeB_4. It indicates that FeB_4 is easier to deform under both shear stress and normal compressive pressure in (Vickers) indentation tests, and is thus likely to be softer than CrB_4. Our ideal strength calculations will explore the stress response at large strains and assess whether there is a strain-stiffening effect that could produce the anomalously high indentation hardness reported in the recent experiment [1].

TABLE I. The calculated lattice constants (a,b,c) in Å, bulk (B) and shear (G) moduli in GPa, and Poisson's ratio (ν), as well elastic constants (C_{ij}) in GPa for FeB_4, in comparison with the previous calculation and CrB_4.

FeB_4	a	b	c		B	G	ν	
	4.522	5.284	3.006		284	194	0.221	
	4.524	5.284	3.004		277	186[a]		
C_{11}	C_{22}	C_{33}	C_{12}	C_{13}	C_{23}	C_{44}	C_{55}	C_{66}
408	754	456	153	159	153	218	148	223
408	754	448	165	160	154	219	141	229[a]
CrB_4	a	b	c		B	G	ν	
	4.723	5.474	2.851		263	267	0.121[b]	
C_{11}	C_{22}	C_{33}	C_{12}	C_{13}	C_{23}	C_{44}	C_{55}	C_{66}
542	855	492	50	104	87	252	280	253[b]

[a]Reference [15].
[b]Reference [21].

III. RESULTS AND DISCUSSION

In Fig. 1, we plot the calculated total electronic density of states (DOS) and partial DOS (PDOS) of FeB_4 at its equilibrium structure, together with the unit cell and crystalline directions of FeB_4 used in the calculations. The results in Figs. 1(b)–1(d) indicate that the s and p states of each B atom hybridize into an sp^3 orbital and form strong covalent B-B

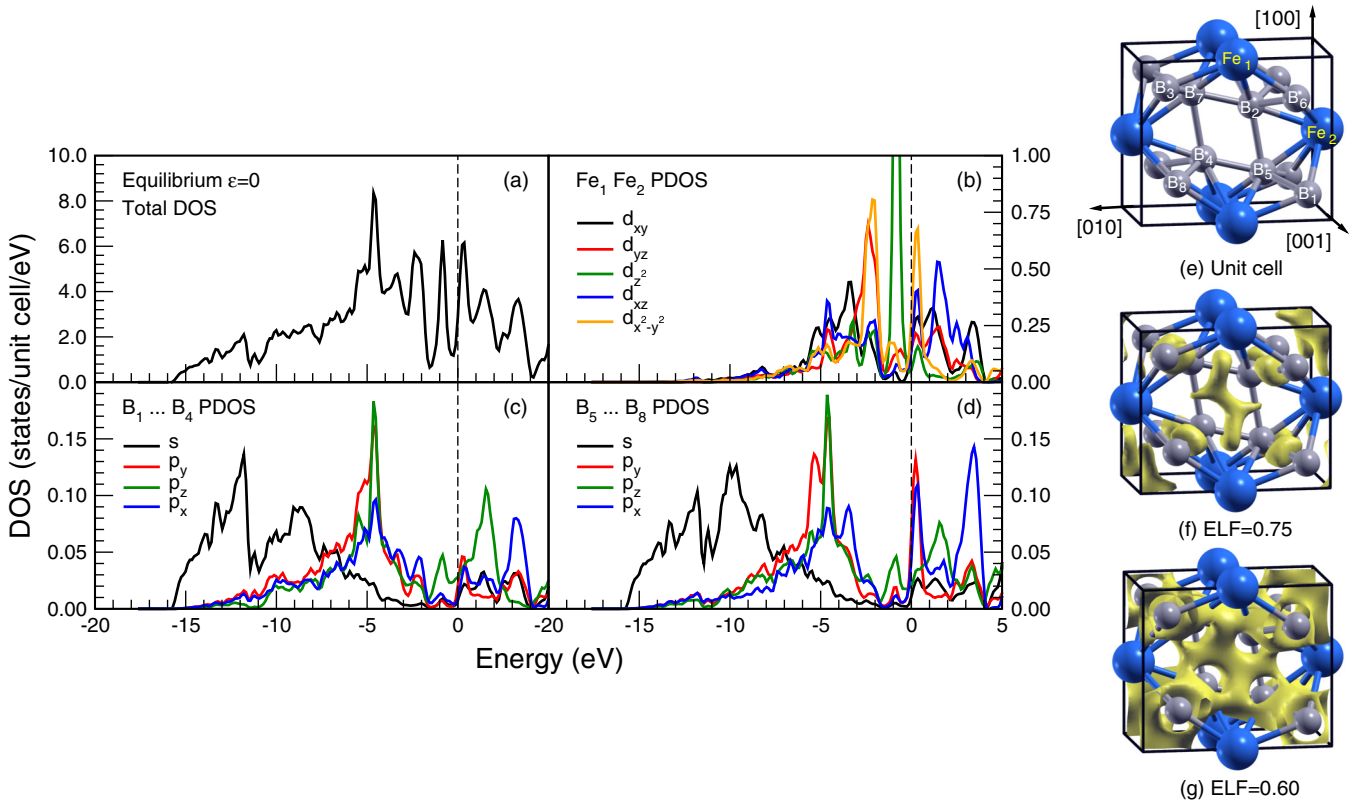

FIG. 1. (Color online) (a)–(d) Calculated total electronic density of states (DOS) and partial DOS (PDOS) of FeB_4 at its equilibrium structure. (e)–(g) The unit cell and crystalline directions of FeB_4, and the calculated isosurface of the electron localization function (ELF) at ELF = 0.75 and 0.6 in its equilibrium structure.

bonds in the energy region of −10 to −3 eV, while the d_{xy} and d_{xz} states of the Fe atoms interact with the three p states of the B atoms in the energy region of −6 to −3 eV, forming less strong covalent Fe-B bonds, which is consistent with the calculated isosurfaces of the electron localization function (ELF), which gives a local measurement of electron paring [43], shown in Figs. 1(f) and 1(g) at ELF = 0.75 (strong covalent B-B bonds) and ELF = 0.6 (less strong covalent Fe-B bonds) in its equilibrium structure. Figure 1(f) also shows clearly the formation of three-centered boron bonds among $\triangle B_5B_2B_4$ and $\triangle B_7B_2B_4$. Such three-center bonding structures have been found in CrB_4 [21] and γ-B_{28} [33], which cause a significant reduction of material strength.

We show in Fig. 2 the calculated stress-strain curves on various shear sliding planes in different inequivalent directions under pure shear deformation for FeB_4. The weakest shear crystalline plane is the (110) plane with the lowest pure shear peak stress of 24.1 GPa appearing along the (110)[001] shear direction [see Fig. 2(e)], which is much lower than the lowest pure shear peak stress of 36.7 GPa appearing in the (110)[1$\bar{1}$0] shear direction in CrB_4 [21]. In Fig. 3, we show the calculated stress-strain curves on various shear sliding planes in different inequivalent directions under (Vickers) indentation shear deformations for FeB_4. The obtained values on all crystalline planes are lower than 40 GPa, with the lowest peak (16.6 GPa) appearing in the (011)[100] direction [see Fig. 3(g)]. This ideal indentation strength value is much lower than that (27 GPa) of CrB_4 [21]. The peak stress in the (011)[100] direction under pure shear deformation is 38 GPa [see Fig. 2(g)]. There is a significant (more than 55%) reduction of the shear strength of FeB_4 in the (011)[100] direction due to the normal compressive pressure in the Vickers indentation.

To understand the large reduction of shear strength in FeB_4 under the (Vickers) indentation shear deformation, we examine the situation of two key shear directions. First, we analyze the stress response of FeB_4 under the (001)[100] shear deformation, in which the peak stress reduces from 44.3 GPa at $\epsilon = 0.35$ under the pure shear to 23.7 GPa at $\epsilon = 0.245$ under the (Vickers) indentation shear deformation. In Fig. 4 we plot the calculated PDOS of boron atoms of FeB_4 at equilibrium $\epsilon = 0$ [see Figs. 4(a) and 4(b)], under the (001)[100] pure shear at $\epsilon = 0.275$ [see Figs. 4(c) and 4(d)], and under Vickers indentation shear at $\epsilon = 0.275$ [see Figs. 4(e) and 4(f)], together with the corresponding structural snapshots of FeB_4 with ELF isosurfaces at ELF = 0.75 [see Figs. 4(g)–4(i)]. Under the (001)[100] pure shear deformation, the electronic states of the B atoms in FeB_4 do not change very much, where the three p states on each B atom remain interacting with its s state in the energy region of −10 to −3 eV [see Figs. 4(c) and 4(d)] hybridizing into an sp^3 orbital and forming B-B bonds among different B atoms, for instance, the B_1-B_5 and B_5-B_9 bonds shown in Figs. 4(g) and 4(h). Under the (001)[100] (Vickers) indentation shear deformation, however, the normal pressure beneath the indenter compresses the structure and induces large lateral expansion in the [100] direction [see Fig. 4(i)]. The shear deformation along the

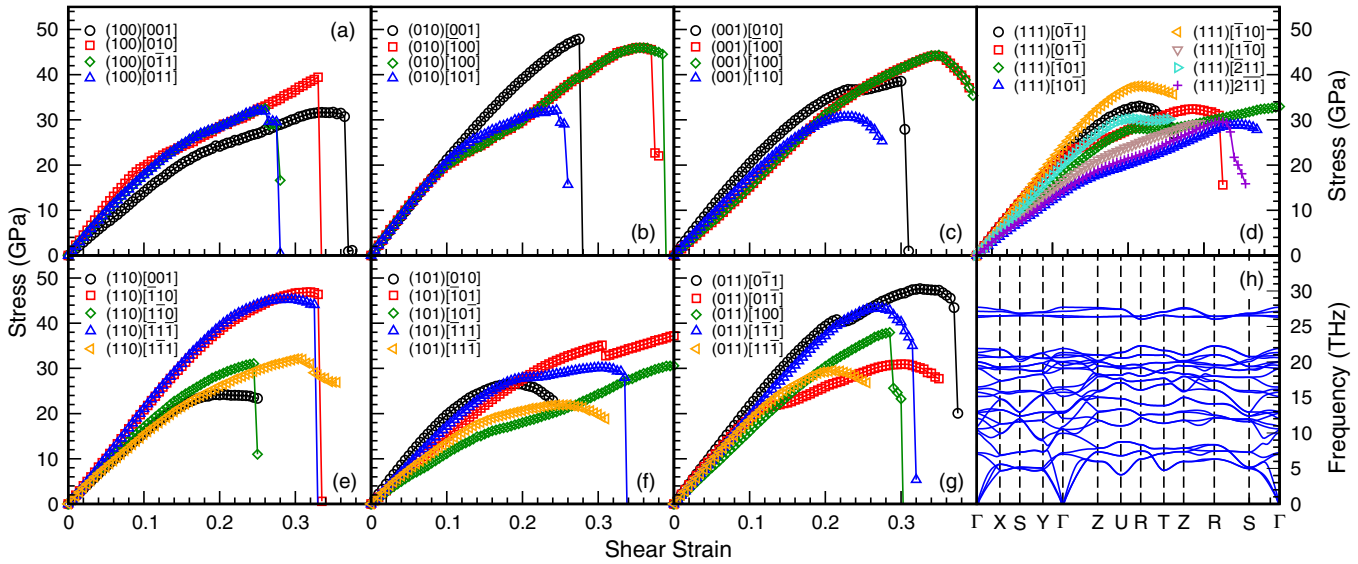

FIG. 2. (Color online) (a)–(g) The calculated stress-strain curves on various shear sliding planes in different directions under pure shear deformation for FeB_4. (h) The calculated phonon bands of FeB_4 at the equilibrium structure.

(001)[100] direction and the lateral structural expansion in the [100] direction driven by the normal compressive pressure beneath the indenter stretches the B_5-B_9 bond (from 1.842 Å at $\epsilon = 0$ to 2.004 Å at $\epsilon = 0.275$); meanwhile the normal pressure in the [001] direction also compresses the B_1-B_5 bond (from 1.842 Å at $\epsilon = 0$ to 1.722 Å at $\epsilon = 0.275$) and reduces significantly the bond angle $\angle B_1B_5B_9$ (from 109.4° at $\epsilon = 0$ to 82.0° at $\epsilon = 0.275$). These local changes around each B atom modify its sp^3 orbital configuration. From Figs. 4(e) and 4(f) one can see that the p_z state of the B atom is pushed to a higher energy region, and its hybridization with the s state of the B atom is reduced, which weakens the covalent bonding between B_5-B_9, indicated by the disappearance of the ELF = 0.75 isosurface between B_5-B_9 [see Fig. 4(i)], and eventually causing the shear stress peak decrease from 44.3 GPa (at $\epsilon = 0.35$) under the (001)[110] pure shear to 23.7 GPa (at $\epsilon = 0.245$) under the (Vickers) indentation shear deformation.

In the above stress-strain calculations, we adopted a non-spin-polarized configuration for the Fe atoms in FeB_4, which has been tested to be correct for its equilibrium structure in the present and previous works [2]. Under indentation shear deformations, however, magnetization of the Fe atoms may appear during the structural changes. In Fig. 5, we plot the stress-strain curves calculated with spin-polarized configurations by assuming that the magnetic moments of the two Fe atoms in the unit cell of FeB_4 [see Fig. 1(e)] to be parallel [ferromagnetic (FM)] and antiparallel [antiferromagnetic (AFM)] at each

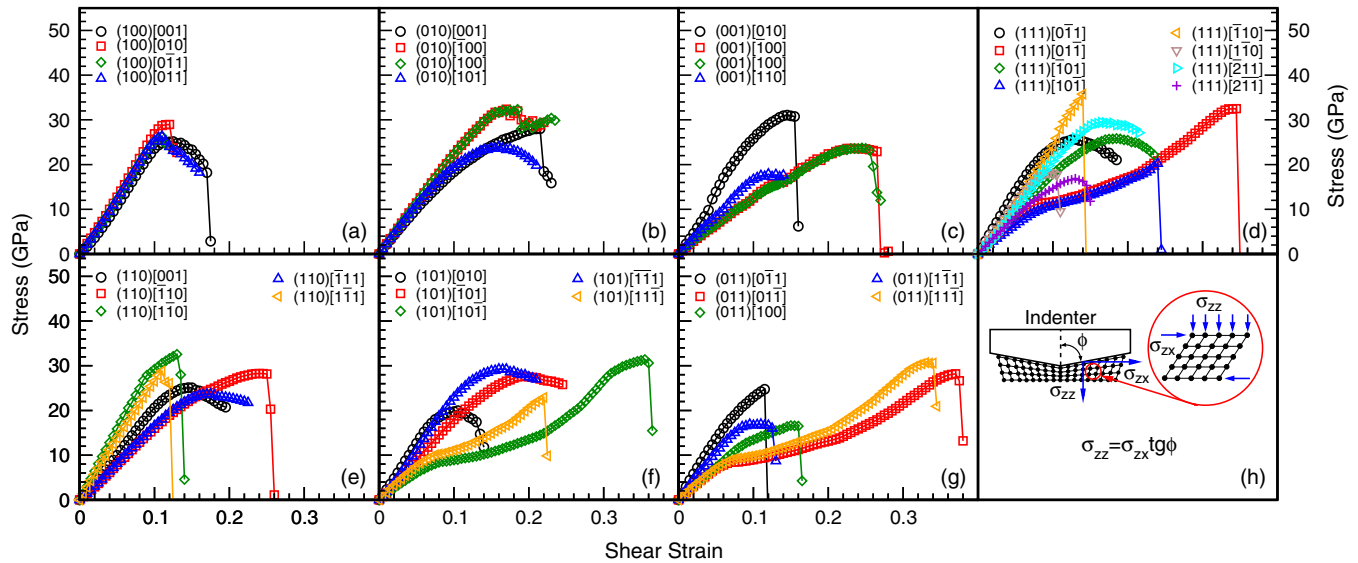

FIG. 3. (Color online) (a)–(g) The calculated stress-strain curves on various shear sliding planes in different directions under Vickers indentation shear deformation for FeB_4. (h) A sketch of indentation stress conditions.

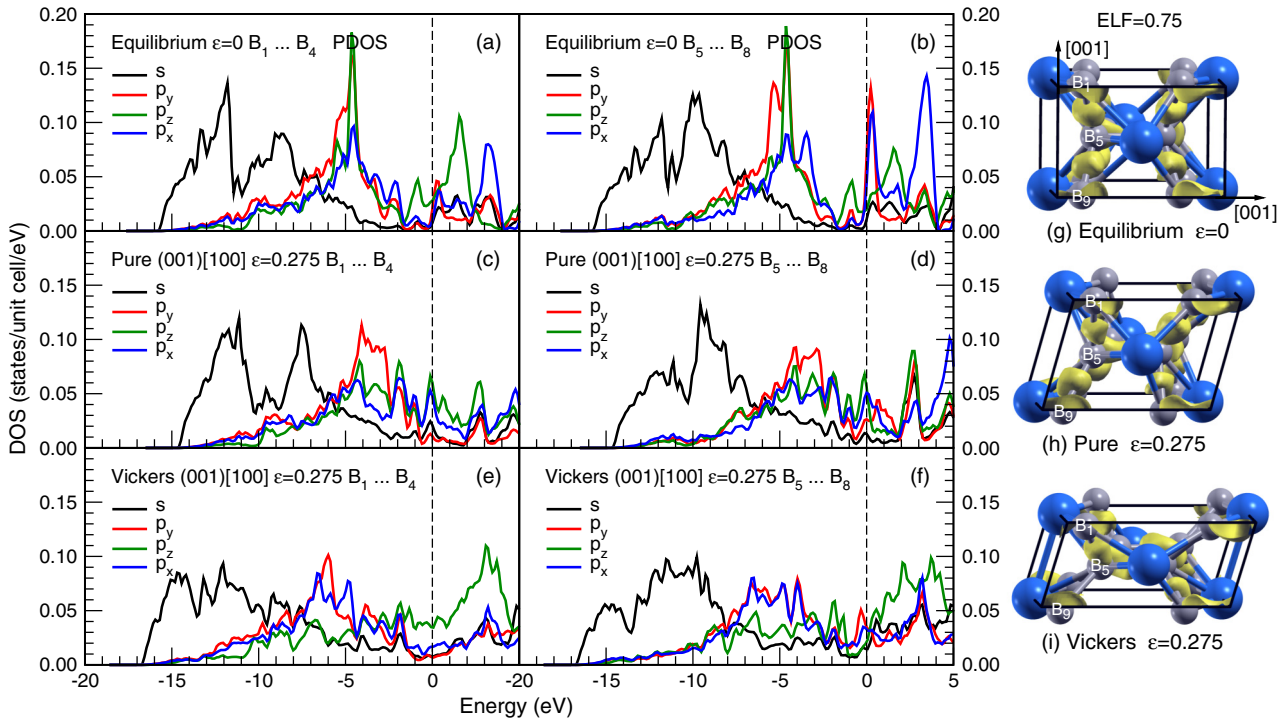

FIG. 4. (Color online) The calculated partial DOS of boron atoms of FeB_4 (a), (b) at equilibrium $\epsilon = 0$; (c), (d) under (001)[100] pure shear at $\epsilon = 0.275$; and (e), (f) under Vickers indentation shear at $\epsilon = 0.275$. Also given in (g)–(i) are the corresponding structural snapshots of FeB_4 with ELF isosurfaces at ELF = 0.75.

relaxation step in the (001)[100] (Vickers) indentation shear deformation, with the initial magnetic moment for each Fe atom set to be $5\mu_B$ (Bohr magneton). A PBE+U scheme is also used in the calculation with the parameter U fixed at 0.4 eV. We used $U = 0.4$ eV in our calculations following the previous work where various kinds of exchange-correlation functionals were tested to interpret the structural, magnetic, and hyperfine properties of Fe_4N, and identified PBE+U with $U = 0.4$ eV as the most accurate exchange-correlation functional for Fe in this material [44]. The results show that a magnetic moment of about $0.8\mu_B$ appears and then disappears on each Fe atom during the (Vickers) indentation shear deformation, but the magnetization of the Fe atoms has little impact on the stress and energy of FeB_4 [the energy increase with the PBE+U results in Fig. 5(b) comes from the addition of the U parameter]. Different values of U ranging from 3.7 to 4.3 eV have also been used for Fe in different iron compounds [45,46]. So we carried out additional calculations with $U = 1$, 2, 4 eV for FeB_4 with its initial magnetic states assumed to be non-, ferro-, and antiferromagnetic at each step under (001)[100] (Vickers) indentation shear deformation. Our results show that with $U = 2$ and 4 eV, the equilibrium structure of FeB_4 becomes ferromagnetic even when we assumed the magnetic moments of iron atoms to be equal to zero in the initial state before structural relaxations. This is inconsistent with the experimental results where a diamagnetic state was found for the equilibrium structure of FeB_4 [1]. So we calculated only the stress-strain relations for FeB_4 with $U = 1$ eV. The results indicate (not shown here) that the indentation strength (the stress peak) is not affected by the choice of different U values.

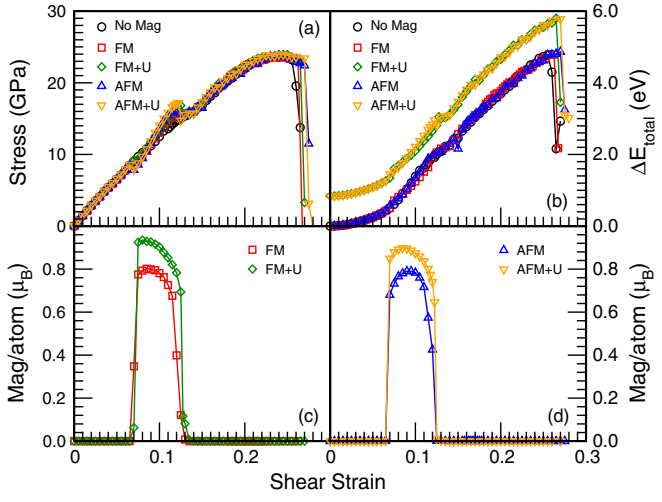

FIG. 5. (Color online) (a), (b) The calculated stress and energy difference (relative to that at equilibrium) of FeB_4 under (001)[100] Vickers indentation shear with no magnetization, ferromagnetization (and plus U), and antiferromagnetization (and plus U) configurations ($U = 0.4$ eV). (c), (d) The calculated magnetic moment (in units of μ_B) of the iron atoms of FeB_4 with ferromagnetization (and plus U) and antiferromagnetization (and plus U) configurations ($U = 0.4$ eV). In ferromagnetization, the magnetic moments of the two iron atoms in the unit cell are equal to each other, while in antiferromagnetization, they are opposite in signs.

We now turn to the analysis of the stress response of FeB_4 under the (011)[100] shear deformation, in which the peak stress reduces from 38.0 GPa at $\epsilon = 0.285$ under the pure shear to 16.6 GPa (the lowest peak stress) at $\epsilon = 0.15$ under

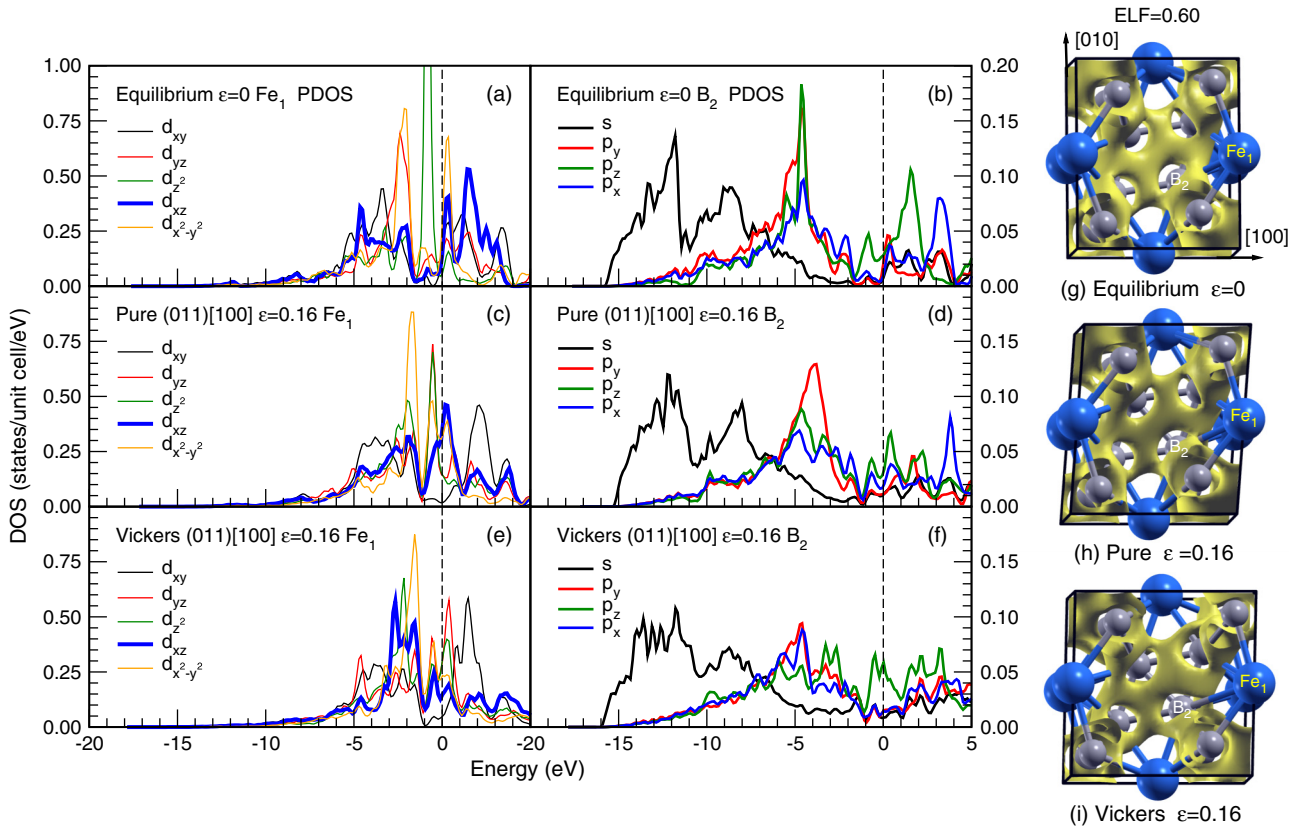

FIG. 6. (Color online) The calculated partial DOS of selected iron and boron atoms of FeB_4 (a), (b) at equilibrium $\epsilon = 0$; (c), (d) under (011)[100] pure shear at $\epsilon = 0.16$; and (e), (f) under Vickers indentation shear at $\epsilon = 0.16$. Also given in (g)–(i) are the corresponding structural snapshots of FeB_4 with ELF isosurfaces at ELF = 0.6.

the (Vickers) indentation shear deformation. In Fig. 6 we plot the calculated PDOS of selected iron (Fe_1) and boron (B_2) atoms of FeB_4 at equilibrium $\epsilon = 0$ [see Figs. 6(a) and 6(b)], under the (011)[100] pure shear at $\epsilon = 0.16$ [see Figs. 6(c) and 6(d)], and under Vickers indentation shear at $\epsilon = 0.16$ [see Figs. 6(e) and 6(f)], together with the corresponding structural snapshots of FeB_4 with ELF isosurfaces at ELF = 0.60 [see Figs. 6(g)–6(i)]. Under the (011)[100] pure shear deformation, the electronic states of the Fe_1 and B_2 atoms in FeB_4 do not change very much, where the d_{xz} state of Fe_1 and the p states of B_2 remain interacting in the energy region of -6 to -2 eV [see Figs. 6(c) and 6(d)] forming the covalent Fe_1-B_2 bond shown in Figs. 6(g) and 6(h). Under the (011)[100] (Vickers) indentation shear deformation, however, the normal pressure beneath the indenter compresses the structure and induces a lateral expansion in the [100] direction [see Fig. 6(i)]. The shear deformation along the (011)[100] direction and the lateral structural expansion in the [100] driven by the normal compressive pressure beneath the indenter stretches the Fe_1-B_2 bond (from 2.250 Å at $\epsilon = 0$ to 2.590 Å at $\epsilon = 0.16$), which pushes the d_{xz} state of Fe_1 to a higher energy region (-3 to -1 eV), weakening its hybridization with the p states of the B_2 atom to form the covalent bond between Fe_1-B_2, as indicated by the disappearance of the ELF = 0.60 isosurface between Fe_1-B_2 [see Fig. 6(i)], and eventually causing the shear stress peak to decrease from 38.0 GPa (at $\epsilon = 0.285$) under the (011)[100] pure shear to 16.6 GPa (at $\epsilon = 0.15$) under the (Vickers) indentation shear deformation. In fact, such an early breaking of boron bonds induced by the lateral expansion under (Vickers) indentation shear deformation is a systematic trend that has been found in other TM-B compounds, such as ReB_2 [20], WB_3 [37], MoB_3 [37], and CrB_4 [21], limiting their indentation strength to below 30 GPa.

IV. CONCLUSIONS

We have performed systematic first-principles calculations to examine the pure shear and indentation shear strength of FeB_4. Our results show that the fundamental constraints limiting the strength and hardness of TM-B compounds also apply to FeB_4. The normal pressure beneath the indenter drives a lateral structural expansion which further stretches and weakens the boron-boron and boron-iron bonds in addition to that caused by the shear deformation in Vickers indentation tests. This effect leads to considerably reduced strength of FeB_4, producing an ideal (i.e., an upper bound) indentation strength of about 17 GPa, which is lower than that (27 GPa) predicted for CrB_4 and much lower than the reported measured Vickers hardness (62 GPa) of FeB_4. Our calculation results are consistent with previous reports of lower shear modulus and large Poisson's ratio of FeB_4 compared to CrB_4, indicating FeB_4 is easier to deform and thus softer under both shear stress and normal compressive pressure in (Vickers) indentation loadings. More important, our calculations show that there is

no strain-stiffening effect in FeB_4 under indentation. These results offer compelling evidence indicating that FeB_4 is unlikely to be superhard, and the mechanical properties of FeB_4 are expected to be in line with other TM-B compounds. Our theoretical study suggests that the hardness of FeB_4 needs to be reexamined by further experimental investigations.

ACKNOWLEDGMENTS

This work was supported by DOE (DE-NA0001982) at UNLV and NNSF of China (No. 11174200) at SJTU. H.S. appreciates the support of the Science and Engineering Interdisciplinary Research Foundation of SJTU.

[1] H. Y. Gou, N. Dubrovinskaia, E. Bykova, A. A. Tsirlin, D. Kasinathan, W. Schnelle, A. Richter, M. Merlini, M. Hanfland, A. M. Abakumov, D. Batuk, G. Van Tendeloo, Y. Nakajima, A. N. Kolmogorov, and L. Dubrovinsky, Phys. Rev. Lett. **111**, 157002 (2013).
[2] A. N. Kolmogorov, S. Shah, E. R. Margine, A. F. Bialon, T. Hammerschmidt, and R. Drautz, Phys. Rev. Lett. **105**, 217003 (2010).
[3] R. B. Kaner, J. J. Gilman, and S. H. Tolbert, Science **308**, 1268 (2005).
[4] H. Y. Chung, M. B. Weinberger, J. B. Levine, A. Kavner, J. M. Yang, S. H. Tolbert, and R. B. Kaner, Science **316**, 436 (2007).
[5] J. B. Levine, S. L. Nguyen, H. I. Rasool, J. A. Wright, S. E. Brown, and R. B. Kaner, J. Am. Chem. Soc. **130**, 16953 (2008).
[6] A. Latini, J. V. Rau, D. Ferro, R. Teghil, V. R. Albertini, and S. M. Barinov, Chem. Mater. **20**, 4507 (2008).
[7] Q. Gu, G. Krauss, and W. Steurer, Adv. Mater. **20**, 3620 (2008).
[8] J. Q. Qin, D. W. He, J. H. Wang, L. M. Fang, L. Lei, Y. J. Li, J. A. Hu, Z. L. Kou, and Y. Bi, Adv. Mater. **20**, 4780 (2008).
[9] N. Orlovskaya, Z. L. Xie, M. Klimov, H. Heinrich, D. Restrepo, R. Blair, and C. Suryanarayana, J. Mater. Res. **26**, 2772 (2011).
[10] R. Mohammadi, A. T. Lech, M. Xie, B. E. Weaver, M. T. Yeung, S. H. Tolbert, and R. B. Kaner, Proc. Natl. Acad. Sci. U.S.A. **108**, 10958 (2011).
[11] C. Liu, F. Peng, N. Tan, J. Liu, F. Li, J. Qina, J. Wang, Q. Wang, and D. He, High Pressure Res. **31**, 275 (2011).
[12] M. Xie, R. Mohammadi, Z. Mao, M. M. Armentrout, A. Kavner, R. B. Kaner, and S. H. Tolbert, Phys. Rev. B **85**, 064118 (2012).
[13] H. Niu, J. Wang, X. Q. Chen, D. Li, Y. Li, P. Lazar, R. Podloucky, and A. N. Kolmogorov, Phys. Rev. B **85**, 144116 (2012).
[14] A. Knappschneider, C. Litterscheid, D. Dzivenko, J. A. Kurzman, R. Seshadri, N. Wagner, J. Beck, R. Riedel, and B. Albert, Inorg. Chem. **52**, 540 (2013).
[15] X. Y. Zhang, J. Q. Qin, J. L. Ning, X. W. Sun, X. T. Li, M. Z. Ma, and R. P. Liu, J. Appl. Phys. **114**, 183517 (2013).
[16] C. Jiang and S. G. Srinivasan, Nature (London) **496**, 339 (2013).
[17] Z. C. Pan, H. Sun, and C. F. Chen, Phys. Rev. Lett. **98**, 135505 (2007).
[18] Z. C. Pan, H. Sun, and C. F. Chen, Phys. Rev. B **79**, 104102 (2009).
[19] Z. C. Pan, H. Sun, Y. Zhang, and C. F. Chen, Phys. Rev. Lett. **102**, 055503 (2009).
[20] C. Zang, H. Sun, J. S. Tse, and C. Chen, Phys. Rev. B **86**, 014108 (2012).
[21] B. Li, H. Sun, C. P. Zang, and C. F. Chen, Phys. Rev. B **87**, 174106 (2013).
[22] D. Roundy, C. R. Krenn, M. L. Cohen, and J. W. Morris, Jr., Phys. Rev. Lett. **82**, 2713 (1999).
[23] H. Chacham and L. Kleinman, Phys. Rev. Lett. **85**, 4904 (2000).
[24] S. H. Jhi, S. G. Louie, M. L. Cohen, and J. W. Morris, Jr., Phys. Rev. Lett. **87**, 075503 (2001).
[25] S. Ogata, J. Li, and S. Yip, Science **298**, 807 (2002).
[26] D. M. Clatterbuck, C. R. Krenn, M. L. Cohen, and J. W. Morris, Jr., Phys. Rev. Lett. **91**, 135501 (2003).
[27] X. Blase, P. Gillet, A. San Miguel, and P. Mélinon, Phys. Rev. Lett. **92**, 215505 (2004).
[28] Y. Zhang, H. Sun, and C. F. Chen, Phys. Rev. Lett. **93**, 195504 (2004).
[29] Y. Zhang, H. Sun, and C. F. Chen, Phys. Rev. Lett. **94**, 145505 (2005).
[30] M. G. Fyta, I. N. Remediakis, P. C. Kelires, and D. A. Papaconstantopoulos, Phys. Rev. Lett. **96**, 185503 (2006).
[31] J. Yang, H. Sun, and C. F. Chen, J. Am. Chem. Soc. **130**, 7200 (2008).
[32] P. Lazar, X. Q. Chen, and R. Podloucky, Phys. Rev. B **80**, 012103 (2009).
[33] W. Zhou, H. Sun, and C. F. Chen, Phys. Rev. Lett. **105**, 215503 (2010).
[34] J. Li, K. J. Van Vliet, T. Zhu, S. Yip, and S. Suresh, Nature (London) **418**, 307 (2002).
[35] A. Gouldstone, H.-J. Koh, K.-Y. Zeng, A. E. Giannakopoulos, and S. Suresh, Acta Mater. **48**, 2277 (2000).
[36] C. R. Krenn, D. Roundy, M. L. Cohen, D. C. Chrzan, and J. W. Morris, Jr., Phys. Rev. B **65**, 134111 (2002).
[37] C. P. Zang, H. Sun, and C. F. Chen, Phys. Rev. B **86**, 180101(R) (2012).
[38] http://www.vasp.at/.
[39] P. E. Blöchl, Phys. Rev. B **50**, 17953 (1994); G. Kresse and D. Joubert, *ibid.* **59**, 1758 (1999).
[40] J. P. Perdew, K. Burke, and M. Ernzerhof, Phys. Rev. Lett. **77**, 3865 (1996).
[41] M. P. Teter, M. C. Payne, and D. C. Allan, Phys. Rev. B **40**, 12255 (1989); D. M. Bylander, L. Kleinman, and S. Lee, *ibid.* **42**, 1394 (1990).
[42] H. J. Monkhorst and J. D. Pack, Phys. Rev. B **13**, 5188 (1976).
[43] A. D. Becke and K. E. Edgecombe, J. Chem. Phys. **92**, 5397 (1990); B. Silvi and A. Savin, Nature (London) **371**, 683 (1994).
[44] E. L. P. y Blanca, J. Desimoni, N. E. Christensen, H. Emmerich, and S. Cottenier, Phys. Status Solidi B **246**, 909 (2009).
[45] P. Mohn, C. Persson, P. Blaha, K. Schwarz, P. Novak, and H. Eschrig, Phys. Rev. Lett. **87**, 196401 (2001).
[46] P. L. Liao and E. A. Carter, Acta Mater. **58**, 5912 (2010).